



***In situ* assessment of mitochondrial respiratory activity and lipid metabolism of mouse oocytes using resonance Raman spectroscopy**

Journal:	<i>Analyst</i>
Manuscript ID	AN-ART-06-2021-001106.R2
Article Type:	Paper
Date Submitted by the Author:	08-Oct-2021
Complete List of Authors:	Ishigaki, Mika; Kansei Gakuin Daigaku Rikogakubu Daigakuin Rikogaku Kenkyuka, Science and Technology; Shimane University, Faculty of Life and Environmental Science Kashiwagi, Shinsuke; HORIBA, Ltd., Bio/Life Science Project, Sales Division Wakabayashi, Satoru; HORIBA, Ltd., Bio/Life Science Project, Sales Division Hoshino, Yumi; Hiroshima University

1
2
3
4
5
6
7 ***In situ* assessment of mitochondrial respiratory activity and**
8
9 **lipid metabolism of mouse oocytes using resonance Raman**
10 **spectroscopy**
11
12
13
14
15
16

17 Mika Ishigaki^{1,2*}, Shinsuke Kashiwagi³, Satoru Wakabayashi³, Yumi
18
19 Hoshino^{4*}
20
21
22
23
24
25

26 ¹*Institute of Agricultural and Life Sciences, Academic Assembly, Shimane*
27
28 *University, 1060 Nishikawatsu, Matsue, Shimane, 690-8504, Japan*
29
30

31 ²*Raman Project Center for Medical and Biological Applications, Shimane*
32
33 *University, 1060 Nishikawatsu, Matsue, Shimane 690-8504, Japan*
34
35

36 ³*Bio/Life Science Project, Sales Division, HORIBA, Ltd., 2*
37
38 *Miyanohigashi-cho, Kisshoin, Minami-ku, Kyoto 601-8510, Japan*
39
40

41 ⁴*Laboratory of Animal Reproduction, Graduate School of Integrated*
42
43 *Science for Life, Hiroshima University, 1-4-4 Kagamiyama,*
44
45 *Higashi-Hiroshima, Hiroshima 739-8528, Japan*
46
47
48
49

50
51
52
53
54
55 *Authors to whom correspondence should be sent.

56
57
58 *E-mail: ishigaki@life.shimane-u.ac.jp (M.I.)
59
60

1
2
3
4
5
6 hoshinoy@fc.jwu.ac.jp (Y.H.)
7
8
9
10
11

12 **Keywords:** Raman spectroscopy, Resonance Raman spectroscopy, Mouse
13
14
15 oocyte, Mitochondrial respiratory activity, Lipid metabolism
16
17
18
19
20
21
22
23
24
25
26
27
28
29
30
31
32
33
34
35
36
37
38
39
40
41
42
43
44
45
46
47
48
49
50
51
52
53
54
55
56
57
58
59
60

Abstract

This study aimed to develop a method to determine the degree of oocyte maturation in metaphase II *in situ* based on the balance between mitochondrial respiratory activity and lipid metabolism using resonance Raman spectroscopy. A decrease in respiratory activity of overmatured oocytes was indicated by the reduced intensities of the resonance Raman bands corresponding to reduced cytochrome *c* in the cytoplasm. Moreover, the increased lipid concentration in overmature oocytes indicated lower lipid metabolism with decreased mitochondrial function. New indexes were defined in terms of the ratios of the representative Raman peak intensities of reduced cytochrome *c* (750 and 1127 cm^{-1}) to those of lipids (1438 cm^{-1}) and they successfully classify the oocytes into groups based on their quality, which varied with their maturation degree. The high development rate of embryos that were fertilized *in vitro* after laser irradiation showed that laser irradiation was noninvasive to oocytes. The evaluation of two factors *in situ*, the active respiration and lipid metabolism, means to catch the most fundamental biochemical reactions of life activities. Our results demonstrate the potential application of resonance Raman spectroscopy as

1
2
3
4
5
6 a new, noninvasive, and universal cell evaluation technology, for not only
7
8
9 oocyte but also more general cells such as somatic cells and iPS cells.
10
11
12
13
14

15 **Introduction**

16
17
18 Oocyte quality is an intrinsically important factor that affects the success
19
20
21 rate of infertility treatment in humans. A novel technology to assess oocyte
22
23
24 quality is required worldwide. The degree of oocyte maturity is one of the
25
26
27 factors that determines oocyte quality. An oocyte suspends its meiosis in
28
29
30 metaphase II (MII) after ovulation and waits to be fertilized. Even during
31
32
33 the suspension of meiosis, *in ovo* substances change from moment to
34
35
36 moment to adapt to fertilization.¹⁻³ However, the observation of
37
38
39 morphological features, such as the shape of the spindle and the polar body,
40
41
42 under a microscope is currently the only nondestructive means of
43
44
45 determining the optimal fertilization period. Therefore, a novel evaluation
46
47
48 technique is required to assess oocyte quality based on *in situ* molecular
49
50
51 information.
52
53

54 Raman spectra reflect molecular information, such as the
55
56
57 concentration and structure of proteins, lipids, and DNA, and they can be
58
59
60

1
2
3
4
5
6 nondestructively obtained *in situ* without labeling even from complicated
7
8
9 biological systems. Thus, Raman spectroscopy has been actively studied
10
11
12 for its biological and medical applications.⁴⁻⁶ For example, Chan et al. used
13
14
15 single-cell micro-Raman spectroscopy to discriminate neoplastic cells from
16
17
18 human lymphocytes.⁷ The differences in the Raman spectra between DNA
19
20
21 and proteins were used to distinguish normal lymphocytes from neoplastic
22
23
24 lymphocytes. Tan et al. found distinct differences between the Raman
25
26
27 spectra of human induced pluripotent stem (iPS) cells and differentiated
28
29
30 human embryonic stem (ES) cells resulting from changes in intracellular
31
32
33 substances associated with the differentiation of ES cells.⁸ Raman
34
35
36 measurements using a 532-nm excitation wavelength are particularly
37
38
39 suitable for the analysis of cytochromes in living cells. Okada et al.
40
41
42 reported label-free Raman imaging of HeLa cell apoptosis using a 532-nm
43
44
45 excitation.⁹ Kakita et al. used resonance Raman signals obtained from
46
47
48 cytochromes to quantify the reduction states of cytochromes *b* and *c* in
49
50
51 *Saccharomyces cerevisiae* cells.¹⁰

52
53
54 Raman spectroscopy has been used to study oocytes or embryos.¹¹⁻¹⁵
55
56
57 Bogliolo et al. studied aging-related oxidative damage in the mouse MII
58
59
60

1
2
3
4
5
6 phase, and young oocytes were distinguished from old oocytes by
7
8
9 performing a principal component analysis (PCA) of lipid and protein
10
11 Raman bands.¹² Heraud et al. reported the changes of macromolecular
12
13 architecture such as proteins, lipids, and cytochromes in living and fixed
14
15 mouse oocytes during MI, MII, and germinal vesicle phases using a
16
17 532-nm Raman imaging.¹³ In our previous study, we evaluated oocyte
18
19 maturity using a 785-nm excitation.¹⁴ Well-matured oocytes with high
20
21 viability competence were identified based on phosphate Raman bands.¹⁴
22
23 Furthermore, Ishigaki et al. investigated the relationship between
24
25 embryonic morphological features and biomolecular composition.¹⁵ They
26
27 proved that embryos with poor morphology had higher lipid concentrations
28
29 than those with good blastomere features and color.¹⁵
30
31
32
33
34
35
36
37
38
39
40
41

42 In this study, Raman spectroscopy was used to assess the degree of
43
44 oocyte maturation *in situ* at the molecular level. Especially, resonance
45
46 Raman spectra were obtained from living oocytes using a 532-nm
47
48 excitation, which matches the resonance conditions of reduced
49
50 cytochromes *b* and *c*. Raman spectra were obtained *in situ* for four different
51
52 phases of oocyte maturation, and the spectral variations among the phases
53
54
55
56
57
58
59
60

1
2
3
4
5
6 were investigated. Cytochromes *b* and *c* play important roles in
7
8
9
10
11
12
13
14
15
16
17
18
19
20
21
22
23
24
25
26
27
28
29
30
31
32
33
34
35
36
37
38
39
40
41
42
43
44
45
46
47
48
49
50
51
52
53
54
55
56
57
58
59
60

mitochondrial aerobic respiration, and the redox of cytochrome *c* functions to transport electrons within ATP generating process.¹⁶⁻¹⁸ Generally, oxidative damage to cells begins by the excess generation of reactive oxygen species (ROS), which robs the antioxidant capacity, and the intracellular redox balance tilts to an oxidative state.¹⁹⁻²¹ Such an oxidative stress causes mitochondrial dysfunction. The ROS scavenging ability decreases with aging and oocytes are injured by oxidative damage due to ovary aging and post-ovulatory aging.^{22, 23} Therefore, mitochondrial function can be evaluated by investigating redox state of cytochrome *c*. Multivariate analysis such as PCA and multi curve resolution (MCR) of the resonance Raman spectra was used to qualitatively and quantitatively evaluate the change in the relative proportions of the reduced and oxidized cytochrome states. The decrease in respiratory activity was identified by measuring the decrease in the intensity of the resonance Raman signals corresponding to reduced cytochrome *c* over the course of overmaturation. Furthermore, the decrease in lipid metabolism was also determined by detecting the increase in the intensity of Raman signals due to lipids. We

1
2
3
4
5
6 defined new indexes to reflect the balance between the decrease in
7
8
9 respiratory activity and lipid accumulation, I_{750}/I_{1438} and I_{1127}/I_{1438} ,
10
11
12 which denote the ratios of the representative Raman peak intensities of
13
14
15 reduced cytochrome *c* (750 and 1127 cm^{-1}) to those of lipids (1438 cm^{-1}),
16
17
18 and we defined the product of these two ratios as a new parameter to assess
19
20
21 the oocyte quality. This parameter successfully classified the oocytes based
22
23
24 on their quality, which varied with their degree of maturation. Furthermore,
25
26
27 *in vitro* fertilization was performed on oocytes after 15 s of laser irradiation
28
29
30 (with a 532-nm excitation and 7.0-mW laser power at the sampling point
31
32
33 by continuously scanning the laser spot across a circular area with a 5- μm
34
35
36 diameter), and the effect of the laser was evaluated from the developmental
37
38
39 rate for the morula and blastocyst stages. The results showed that the
40
41
42 Raman measurements were noninvasive.
43
44

45
46 These results suggest that Raman spectroscopy can be used to
47
48 noninvasively assess oocyte quality based on the balance between
49
50
51 respiration activity and lipid metabolism. Lipids are potent sources of
52
53
54 cellular energy, and lipid metabolism is closely related to cell respiration
55
56
57 for energy production in the mitochondrial matrix.²⁴⁻²⁶ Therefore, an *in situ*
58
59
60

1
2
3
4
5
6 assessment of cell activity based on the balance between respiration
7
8 activity and lipid metabolism has potential application to somatic cells and
9
10 iPS cells, in addition to oocytes. This study may provide a new general
11
12 method for evaluating cell activity *in situ*.
13
14
15
16
17
18
19
20

21 **Materials and Methods**

22 **Animals and oocyte collection**

23
24 ICR mice were purchased from Japan SLC Inc. (Shizuoka, Japan).
25
26 Immature 20- to 23-day-old female mice were used. An ovulation treatment
27
28 was performed using 5 IU pregnant mare's serum gonadotropin (PMSG;
29
30 Teikoku Hormone MFG, Tokyo, Japan), followed by 5 IU human chorionic
31
32 gonadotropin (hCG; Teikoku Hormone MFG) after 48 h. Oocytes were
33
34 collected from three female mice at each phase (13, 15, 18 and 24 h after
35
36 hCG injection), and the four phases were denoted as Phases I, II, III and
37
38 IV. The experimental design followed that of Sakai et al.²⁷⁻²⁹; the oocytes
39
40 had the highest developmental competence in Phase II and were
41
42 overmatured in Phase IV. The variation in developmental competence over
43
44 the course of oocyte maturation is shown in Figure 1. The oocytes were
45
46
47
48
49
50
51
52
53
54
55
56
57
58
59
60

1
2
3
4
5
6 placed in Leibovitz's L-15 medium (Invitrogen, Grand Island, NY, USA)
7
8
9 containing 0.1% polyvinyl alcohol (PVA; Sigma-Aldrich, St. Louis, MO,
10
11
12 USA). The cumulus cells were removed by treatment with 0.1%
13
14
15 hyaluronidase at 37 °C. The reproducibility was confirmed by repeating the
16
17
18 experimental procedure three times.
19
20
21
22
23

24 **In vitro fertilization and embryo culture**

25
26
27 In vitro fertilization and embryo culture were carried out following
28
29
30 previously reported methods^{14, 30}. Spermatozoa were collected from the
31
32
33 cauda epididymis and preincubated for 2 h in 400 µL of HTF medium to
34
35
36 enable capacitation before insemination. After capacitation, the
37
38
39 spermatozoa were introduced into 200-µL droplets of the fertilization
40
41
42 medium at a final concentration of 700 spermatozoa/µL. At 4 h after
43
44
45 insemination, the penetration of sperm into the oocytes was confirmed by
46
47
48 microscopic examination; the oocytes were subsequently washed
49
50
51 thoroughly five times and then cultured in KSOM medium. All the
52
53
54 embryos were incubated in 100-µL droplets of the culture medium in a
55
56
57 humidified atmosphere of 5% CO₂ in air at 37 °C.
58
59
60

1
2
3
4
5
6 All the experiments were carried out in accordance with the
7
8
9 fundamental guidelines for the proper conduct of animal experiments and
10
11
12 related activities in academic research institutions under the jurisdiction of
13
14
15 the Ministry of Education, Culture, Sports, Science and Technology in
16
17
18 Japan. The present study was approved by the Ethics Committee of
19
20
21 Hiroshima University and Horiba, Ltd. in Japan.
22
23
24
25
26

27 **Raman measurement and multivariate analysis**

28
29
30 The micro Raman system (LabRAM HR Evolution Raman microscope,
31
32
33 Horiba, Kyoto Japan) consisted of a 532-nm DPSS laser, a spectrometer, a
34
35
36 600-gr/mm holographic grating blazed at 500 nm, an EMCCD scientific
37
38
39 camera (SynapseEM, Horiba), and a microscope (an Eclipse Ti2 inverted
40
41
42 microscope, Nikon, Tokyo, Japan) with a 60 × water emersion objective
43
44
45 lens (NA=1.20, Nikon). The excitation laser power was approximately 7.0
46
47
48 mW at the sampling point, and the exposure time was 15 s (15 s × 1).
49
50
51 The system was equipped with a stage-top chamber (BLAST Inc.,
52
53
54 Kanagawa, Japan), within which the oocytes were maintained in the L-15
55
56
57 medium containing 0.1% PVA at 37 °C during each Raman measurement.
58
59
60

1
2
3
4
5
6
7
8
9
10
11
12
13
14
15
16
17
18
19
20
21
22
23
24
25
26
27
28
29
30
31
32
33
34
35
36
37
38
39
40
41
42
43
44
45
46
47
48
49
50
51
52
53
54
55
56
57
58
59
60

Photothermal damage to the oocytes by laser irradiation was prevented by using a DuoScan™ imaging system (Horiba) to continuously scan the laser spot across a specified circular area (diameter: 5 μm) to obtain an averaged oocyte spectrum. The numbers of oocytes measured at each maturation phase were 44 (I), 58 (II), 59 (III), and 57 (V), and one point at the central part of oocytes was measured for each one, where is relatively uniform with few organelles. The measured Raman spectra were calibrated using the peak for silicon. The wavenumber resolution was 2 cm^{-1} , and the autofluorescence background of the sample was removed using 5th-order polynomial fitting. The spectral intensity was normalized by the standard peak at 1001 cm^{-1} for phenylalanine so that the peak height became 1. The averaged Raman spectra for each developmental stage were calculated from the preprocessed Raman data. PCA was carried out using Unscrambler X 10.3 chemometrics software (Camo Analytics, Oslo, Norway). MCR was performed using an open source of nonnegative matrix factorization, a machine learning library “scikit-learn” (ver. 0.21.1) opened by Python (ver. 3.6.1). After guessing the number of effective components by singular value decomposition (SVD) analysis and confirming that

1
2
3
4
5
6 Raman matrix was decomposed into independent pure components, the
7
8
9 MCR calculations were carried out using ingredient and trial numbers of 5
10
11
12 and 1000, respectively. An unpaired two-sided Student's t-test was
13
14
15 performed on the data set for every two phases to identify significant
16
17
18 differences between the pure component concentrations extracted by MCR.
19
20
21
22
23

24 **Sample preparation of cytochromes and resonance Raman** 25 26 27 **measurements**

28
29
30 Cytochrome *b* (C1427, human, Sigma-Aldrich) and cytochrome *c*
31
32 (9007-43-6, from an equine heart, Sigma-Aldrich) reagents were diluted
33
34 with 0.05 M Tris-HCl buffer (pH=7.6, FUJIFILM Wako Pure Chemical
35
36 Co., Osaka, Japan) to a final concentration of 4 μ M. Cytochrome reduction
37
38 was carried out by adding sodium dithionite at final concentrations of 2
39
40 mM and 50 μ M to cytochrome *b* and *c* solutions, respectively. UV-Vis
41
42 absorbance spectra were obtained before each Raman measurement to
43
44 determine whether the cytochromes were in oxidized or reduced states. A
45
46 spectrophotometer (Duetta spectrofluorometer, Horiba) was used to
47
48 perform the UV-Vis measurements in the 375–650 nm region. The Raman
49
50
51
52
53
54
55
56
57
58
59
60

1
2
3
4
5
6 spectra for standard cytochrome solutions were recorded using an XploRA
7
8 Raman microscope (Horiba) equipped with an extension for macro
9
10 measurement, a 10x objective lens (NA=0.25, Olympus, Tokyo, Japan) and
11
12 a grating (1800 gr/mm). A 532-nm excitation wavelength was used, the
13
14 laser power at the sampling point was 11.0 mW, and the exposure time was
15
16 120 s (60 s \times 2).
17
18
19
20
21
22
23
24
25
26

27 **Results and Discussion**

28
29
30 Figure 2 shows the averaged Raman spectra in the 1800–600 cm^{-1} region
31
32 obtained for mouse oocytes at Phases I (n=44), II (n=58), III (n=59), and
33
34 IV (n=57) after the injection of hCG hormone. Distinct peaks from
35
36 proteins, lipids, DNA/RNA, and especially cytochromes can be observed.
37
38 The peak at 1001 cm^{-1} is associated with phenylalanine ring breathing³¹,
39
40 and the corresponding peak height was used as an internal standard to
41
42 normalize the Raman spectra. The band at 1656 cm^{-1} is the overlap of two
43
44 bands assigned to the amide I modes of proteins and the C=C stretching
45
46 modes of lipids³¹, and the band at 1445 cm^{-1} arises from the C-H
47
48 deformation of lipids, proteins, and carbohydrates. The peaks at 1335 and
49
50
51
52
53
54
55
56
57
58
59
60

1
2
3
4
5
6 1311 cm^{-1} are assigned to the CH_3/CH_2 twisting and bending modes³¹. In
7
8
9
10 addition, four prominent peaks associated with reduced cytochromes are
11
12 observed at 1582, 1311, 1125, and 747 cm^{-1} . The 532 nm excitation
13
14 wavelength matches the absorption energy of reduced cytochromes *b* and *c*,
15
16 and the resonance effect remarkably enhanced the intensities of these
17
18 reduced cytochrome peaks. Table 1 summarizes the peak assignments for
19
20 the Raman spectra obtained for the oocytes.
21
22
23
24
25
26

27
28 The origin of the peaks due to cytochromes, namely, oxidized and
29
30 reduced cytochromes *b* and *c*, were confirmed. Figure 3A shows the
31
32 ultraviolet-visible (UV-Vis) absorbance spectra in the 460-600 nm region
33
34 for oxidized and reduced cytochromes *b* and *c*. As the reduced cytochromes
35
36 exhibited absorption maxima near the laser excitation wavelength (532
37
38 nm), the resonance resulted in very strong Raman signals from the reduced
39
40 cytochromes. The enhancement of the Raman signals from the absorption
41
42 of the oxidized cytochromes deviated from the resonance condition,
43
44 resulting in less enhanced Raman signals. The Raman spectra of reduced
45
46 cytochromes *b* and *c* were characterized by typical strong peaks at
47
48 approximately 1582, 1123, and 750 cm^{-1} (Figure 3B): the peaks at 1123 and
49
50
51
52
53
54
55
56
57
58
59
60

1
2
3
4
5
6 750 cm^{-1} were assigned to pyrrole half-ring (ν_{22}) and pyrrole ring breathing
7
8
9 (ν_{15}) modes, respectively^{31, 32}. The cytochrome *c* spectrum exhibited a
10
11 strong peak at 1312 cm^{-1} , whereas the cytochrome *b* spectrum exhibited
12
13 two peaks at 1338 and 1301 cm^{-1} . A characteristic feature of the
14
15 cytochrome *c* spectra was the appearance of relatively strong peaks at 690
16
17 and 643 cm^{-1} . The abovementioned properties of the resonance Raman
18
19 spectra of cytochromes *b* and *c* confirmed that the strong peaks (1582,
20
21 1311, 1125, and 747 cm^{-1}) in the Raman spectra obtained for mouse
22
23 oocytes at four stages were mainly derived from the reduced cytochromes.
24
25
26
27
28
29
30
31
32
33
34
35

36 **Principal component analysis (PCA)**

37
38
39 The spectral variations were analyzed by PCA to determine how the
40
41 molecular composition changed as the oocytes matured. PCA was
42
43 performed by selecting the most contralateral group of immature (Phase I)
44
45 and overmature (Phase IV) oocytes. Among the combinations of score plots
46
47 of principal components (PCs) in two dimensions, PC 2 vs PC 3 showed
48
49 the best pattern of distinguishing between immature and overmature
50
51 oocytes (Figure 4A). Figure 4B shows the loading plots of PC 1 (55.7%),
52
53
54
55
56
57
58
59
60

1
2
3
4
5
6 PC 2 (12.6%), and PC 3 (3.2%) for the PCA. The loading plot of PC 1
7
8 exhibited strong peaks corresponding to the reduced cytochromes *c*; two
9
10 peaks at 690 and 641 cm^{-1} and a single peak at 1311 cm^{-1} . In the loading
11
12 plot of PC 2, three peaks at 1583, 1127, and 750 cm^{-1} and two peaks at
13
14 1657 and 1438 cm^{-1} appeared in the negative and positive directions,
15
16 respectively. The intensities of the three peaks in the negative direction
17
18 were lower in the overmature phase than in the immature phase. The peak
19
20 in the positive direction at 1657 cm^{-1} was assigned to the amide I mode of
21
22 proteins and the C=C stretching modes of lipids, and the peak at 1438 cm^{-1}
23
24 was assigned to the C-H deformation of proteins, lipids, and hydrocarbons.
25
26 The intensities of these two peaks increased at the overmature phase.
27
28
29
30
31
32
33
34
35
36
37
38

39 The averaged spectral intensities at approximately 1657, 1438, 1127,
40
41 and 750 cm^{-1} for all four phases were compared to confirm the trend in the
42
43 variation in the spectral intensity identified using PCA. The peak intensities
44
45 at 1127 and 750 cm^{-1} were the same for Phases I and II and then gradually
46
47 tended to weaken for Phases III and IV (Figure 4C, 4D) without significant
48
49 differences about the peak positions between them. All the Raman spectra
50
51 were normalized to the phenylalanine peak intensity at 1001 cm^{-1} .
52
53
54
55
56
57
58
59
60

1
2
3
4
5
6 Therefore, the decrease in the cytochrome *c* peak intensities at 1127 and
7
8
9 750 cm^{-1} for Phases III and IV can be interpreted as the deviation of
10
11
12 cytochrome *c* from the reduction state, with a corresponding increase in the
13
14
15 oxidized cytochrome *c* content. The increase in the peak intensities at 1657
16
17
18 and 1438 cm^{-1} suggested an increase in the relative concentration of
19
20
21 molecular compounds other than cytochromes. We previously studied
22
23
24 oocyte maturation using a 785-nm excitation and found that the
25
26
27 concentration of unsaturated fatty acids increased during Phase IV¹⁴.
28
29
30 Characteristic fatty acid peaks at 1658 and 1445 cm^{-1} were extracted from
31
32
33 the high wavenumber region (1800-1400 cm^{-1}) of the spectrum as an index
34
35
36 of overmature oocytes. The two peaks in PC2 appeared at almost the same
37
38
39 position (1657 and 1438 cm^{-1}) in this study as in our previous study and are
40
41
42 attributed to redundant lipids resulting from abnormal lipid metabolism of
43
44
45 overmature oocytes.
46
47
48
49
50

51 **Multi curve resolution (MCR) analysis**

52
53
54 Molecular composition changes during the maturation of oocytes were
55
56
57 semi-quantified using MCR. The spectral data matrix V is a linear
58
59
60

1
2
3
4
5
6 combination $V = WH$, where W and H are matrixes of pure component
7 spectra and its intensity profile, respectively³³. The Raman spectra were
8
9 decomposed into intrinsic components by MCR with a nonnegative
10 restriction, and the corresponding concentration changes were
11
12 quantitatively analyzed. Figure 5A shows the loading plots for the four
13
14 MCR components. Component 1 (C1) is assigned to a protein based on the
15
16 following peaks: the sharp peak at 1001 cm^{-1} corresponds to phenylalanine;
17
18 additional peaks at 742 cm^{-1} arise from tryptophan symmetric breathing
19
20 modes; tyrosine doublets appear at 850 and 828 cm^{-1} ; a C-N stretching peak
21
22 appears at 1124 cm^{-1} ; a broad amide III peak appears at approximately
23
24 1242 cm^{-1} ; twisting and bending modes of CH_3/CH_2 appear in the
25
26 1337-1311 cm^{-1} region; a C-H deformation peak appears at 1446 cm^{-1} ; and
27
28 an amide I peak appears at 1656 cm^{-1} . The detailed Raman peak
29
30 assignments are summarized in Table 1. The spectral pattern of C1 is very
31
32 similar to protein-rich spectra obtained from mouse oocytes at a 785-nm
33
34 excitation¹⁴. Prominent peaks at 1582, 1311, 1126, and 749 cm^{-1} dominated
35
36 C2, which and used in conjunction with peaks at 690 and 641 cm^{-1} to
37
38 assign these spectral components to reduced cytochrome *c*. C3 exhibited
39
40
41
42
43
44
45
46
47
48
49
50
51
52
53
54
55
56
57
58
59
60

1
2
3
4
5
6 the spectral pattern of unsaturated fatty acids, which was exactly the same
7
8
9 as that obtained for the loading plot of PC1 from the PCA used to identify
10
11
12 the overmature oocytes at phase IV in our previous study¹⁴. C4 also
13
14
15 exhibited a cytochrome spectral component. This component was likely to
16
17
18 correspond to reduced cytochrome *b*; the spectral features consist of strong
19
20
21 peaks at 749, 1128, and 1583 cm^{-1} , a broad peak at approximately 1001
22
23
24 cm^{-1} , and double peaks at 1342 and 1314 cm^{-1} . The higher order
25
26
27 components did not show the meaningful spectral pattern due to biological
28
29
30 molecules, and the components up to C4 were enough to be discussed as
31
32
33 the intrinsic components.

34
35
36 C2 and C3 exhibited interesting variations in concentration with
37
38
39 oocyte maturation (Figure 5B). The reduced cytochrome *c* concentration
40
41
42 represented by C2 was high at Phases I and II and decreased as the oocytes
43
44
45 overmatured during Phase IV. The lipid concentration represented by C3
46
47
48 systematically increased with maturation. These results quantitatively show
49
50
51 that overmaturation promoted the oxidation of cytochrome *c*, reduced
52
53
54 respiratory activity, and decreased metabolism, resulting in lipid
55
56
57 accumulation. The MCR results provided a quantitative basis for the
58
59
60

1
2
3
4
5
6 concentration variation in *in ovo* components associated with oocyte
7
8 maturation, which was consistent with the PCA results.
9
10
11
12
13
14

15 **The relationship between respiratory activity and lipid metabolism**

16
17
18 Lipid metabolism and cellular respiration are closely related to each other
19
20 for energy production in the mitochondrial matrix²⁴⁻²⁶. Fatty acids undergo
21
22 β -oxidation, the generated acetyl-CoA is incorporated into the citric acid
23
24 cycle in the mitochondrial matrix, and energy is efficiently produced by
25
26 aerobic breathing³⁴. Carnitine is a vitamin-like substance involved in lipid
27
28 metabolism that functions in transporting fatty acids into mitochondria.
29
30 Somfai et al. reported that L-carnitine treatment increased the density of
31
32 activated mitochondria and that the concentration of lipid droplets
33
34 decreased in porcine oocytes³⁵. Dunning et al. proved that carnitine
35
36 treatment promoted β -oxidation to improve oocyte maturation and
37
38 developmental competence^{19, 36}. These authors mentioned that the
39
40 β -oxidation of fatty acids, especially palmitic acid, was also dramatically
41
42 increased during oocyte maturation. Magnusson et al. reported increased
43
44 oxygen consumption in mature rat oocytes³⁷. That is, enhancement of
45
46
47
48
49
50
51
52
53
54
55
56
57
58
59
60

1
2
3
4
5
6
7
8
9
10
11
12
13
14
15
16
17
18
19
20
21
22
23
24
25
26
27
28
29
30
31
32
33
34
35
36
37
38
39
40
41
42
43
44
45
46
47
48
49
50
51
52
53
54
55
56
57
58
59
60

mitochondrial functions due to the activation of lipid metabolism has been shown to result in good maturation. In this study, we successfully detected the activation of respiration and the improvement of lipid metabolism in well-matured oocytes *in situ*, which are the most fundamental biochemical reactions of life.

New discrimination index of oocyte maturation based on balance between respiratory activity and lipid metabolism

A new index for measuring the oocyte quality *in situ* was proposed based on the observed decrease and increase in the relative concentration of reduced cytochrome *c* and lipids, respectively, resulting from the oxidation of cytochrome *c* and reduced lipid metabolism caused by oocyte overmaturation. The proportion of the peak intensities I_{750}/I_{1438} and I_{1127}/I_{1438} , represented by the ratio of Raman peak intensities due to reduced cytochrome *c* (750 and 1127 cm^{-1}) and lipids (1438 cm^{-1}), were defined as the index reflecting the balance between respiratory activity and lipid metabolism; these indexes were comparatively analyzed over the course of maturation. Figure 6A shows plots of values I_{750}/I_{1438} vs

1
2
3
4
5
6 I_{1127}/I_{1438} values. These two ratios tend to be higher for young oocytes,
7
8
9 which have a higher concentration of reduced cytochrome *c* and lower lipid
10
11
12 accumulation than older oocytes. The data for Phase IV were distributed
13
14
15 away from the data for the other groups on the plot diagonal.
16
17

18
19 A threshold for quantitatively assessing oocyte quality was obtained
20
21 from the frequency distribution of the product of these two indexes
22
23 $(I_{750}/I_{1438} \times I_{1127}/I_{1438})$ (Figure 6B). When both indexes are large, the
24
25 product is also large. If even one of the two indexes is small, the product is
26
27 small, showing that the oocyte is not in good condition, based on the
28
29 respiratory activity and lipid metabolism. The product was scarcely higher
30
31 than one for Phase IV but exceeded one for some data in Phases I and II
32
33 (Figure 6B). The most of the indexes were less than 0.6 for Phase IV. The
34
35 new product index reasonably reproduces the reported trends of oocyte
36
37 quality. A novel evaluation method of oocyte quality can be constructed by
38
39 performing in vitro fertilization after Raman measurement and defining a
40
41 threshold area for the index with a high fertilization rate and high viability.
42
43
44
45
46
47
48
49
50
51
52
53
54
55
56
57
58
59
60

Evaluation of laser invasiveness

1
2
3
4
5
6
7 In vitro fertilization was carried out for laser-irradiated oocytes, and
8
9 embryonic development was observed for five days. Figure 7 shows images
10
11 of (A) laser-irradiated and (B) nonradiated embryos on the fifth day of
12
13 incubation. Several blastocysts and morula were observed, some of which
14
15 were already hatched in both cases.
16
17
18
19

20
21 Figure 7C showed the developmental rates (%) of oocytes that
22
23 progressed to morula or blastocyst stages. The total developmental rate to
24
25 the morula and blastocyst stages in the control was higher than 40% for
26
27 Phases I, II and III. The total developmental rate obtained using the
28
29 ovulation treatment used in this study has been reported to be
30
31 13.4~60.7%²⁷. The oocyte maturation rate followed the same trend as has
32
33 been previously reported, that is, the oocyte maturation rate was highest in
34
35 Phase II and lowest in Phase IV. All the developmental results of the
36
37 control confirmed that oocyte collection was properly carried out.
38
39
40
41
42
43
44
45
46
47

48
49 The laser-irradiated oocytes had a slightly lower developmental rate
50
51 than the control oocytes for Phases I, II and IV. However, the
52
53 developmental rate of laser-irradiated oocytes was higher than those of the
54
55 control oocytes for Phase III. Thus, the effect of laser irradiation on the
56
57
58
59
60

1
2
3
4
5
6 development rate could not be confirmed. Therefore, it was concluded that
7
8
9 laser irradiation had no effect on the oocytes. Invasiveness of the 532-nm
10
11
12 excitation laser on the oocytes was anticipated at the start of the
13
14
15 experiments. Consequently, measures were taken to prevent oocyte
16
17
18 damage: a low irradiation time and power of 15 s and 7.0 mW,
19
20
21 respectively, were used at the sampling points, and the laser irradiation
22
23
24 point was moved within a 5- μ m circle in a zigzag manner. The results
25
26
27 showing the noninvasiveness of the laser irradiation are very useful for
28
29
30 practical application of Raman spectroscopy to the assessment of oocyte
31
32
33 quality.
34
35
36
37
38

39 **Conclusion**

40
41
42 In the present study, we used Raman spectroscopy to evaluate the degree of
43
44
45 oocyte maturation *in situ* by assessing both respiratory activity and lipid
46
47
48 metabolism. The decrease in the intensity of the Raman signal for reduced
49
50
51 cytochrome *c* was used to identify the decrease in respiratory activity in
52
53
54 overmature oocytes; deviation from the resonance condition was caused by
55
56
57 the transition of cytochrome *c* from the reduced state to the oxidized state.
58
59
60

1
2
3
4
5
6 Lipid accumulation was found to occur concomitantly with the decrease in
7
8
9 respiratory activity. Two new indexes were defined to reflect the balance
10
11
12 between decreased respiratory activity and lipid metabolism, i.e. two ratios
13
14 of Raman peak intensities I_{750}/I_{1438} and I_{1127}/I_{1438} , where a value of the
15
16 product of two indexes above one was used to identify oocytes actively
17
18 undergoing respiratory and lipid metabolism. Comparing the
19
20 developmental rate with and without laser irradiation showed that the laser
21
22 had no significant effect on the rate. These results indicate that Raman
23
24 spectroscopy can be used to noninvasively evaluate the oocyte quality *in*
25
26
27
28
29
30
31
32
33
34 *situ* based on respiratory activity and lipid metabolism.

35
36 Both the enhancement of mitochondrial functions and the activation of
37
38 lipid metabolism, which are intrinsically important biochemical reactions
39
40 of life, were successfully detected in this study. An *in situ* assessment of
41
42 cell activity based on the balance between respiration activity and lipid
43
44 metabolism showed that the developed method can be applied to somatic
45
46
47
48
49
50
51
52
53
54
55
56
57
58
59
60 cells and iPS cells, in addition to oocytes. The method may open a new era
for cell evaluation *in situ*.

1
2
3
4
5
6
7
8
9
10
11
12
13
14
15
16
17
18
19
20
21
22
23
24
25
26
27
28
29
30
31
32
33
34
35
36
37
38
39
40
41
42
43
44
45
46
47
48
49
50
51
52
53
54
55
56
57
58
59
60

References

1. I. Hoffmann, P. R. Clarke, M. J. Marcote, E. Karsenti and G. Draetta, *EMBO J.*, 1993, **12**, 53-63.
2. B. Ducommun, P. Brambilla, M. A. Felix, B. R. Franza Jr., E. Karsenti and G. Draetta, *EMBO J.*, 1991, **10**, 3311-3319.
3. M. J. Solomon, T. Lee and M. W. Kirschner, *Mol. Biol. Cell*, 1992, **3**, 13-27.
4. Y. Ozaki, *Appl. Spectrosc. Rev.*, 1988, **24**, 259-312.
5. P. Carey, *Principles of Raman Spectroscopy: Biochemical applications of Raman and resonance Raman spectrometers*. Elsevier, Amsterdam, 2012.
6. L. P. Choo-Smith, H. G. M. Edwards, H. P. Endtz, J. M. Kros, F. Heule, H. Barr, J. S. Robinson Jr., H. A. Bruining and G. J. Puppels, *Biopolymers*, 2002, **67**, 1-9.
7. J. W. Chan, D. S. Taylor, T. Zwerdling, S. M. Lane, K. Ihara and T. Huser, *Biophys. J.*, 2006, **90**, 648-656.
8. Y. Tan, S. O. Konorov, H. G. Schulze, J. M. Piret, M. W. Blades and R. F. Turner, *Analyst*, 2012, **137**, 4509-4515.

- 1
2
3
4
5
6
7
8
9
10
11
12
13
14
15
16
17
18
19
20
21
22
23
24
25
26
27
28
29
30
31
32
33
34
35
36
37
38
39
40
41
42
43
44
45
46
47
48
49
50
51
52
53
54
55
56
57
58
59
60
9. M. Okada, N. I. Smith, A. F. Palonpon, H. Endo, S. Kawata, M. Sodeoka and K. Fujita, *Proc. Natl. Acad. Sci. USA*, 2012, **109**, 28-32.
10. M. Kakita, V. Kaliaperumal and H. O. Hamaguchi, *J. Biophotonics*, 2012, **5**, 20-24.
11. B. Davidson, A. A. Murray, A. Elfick and N. Spears, *PloS One*, 2013, **8**, e67972.
12. L. Bogliolo, O. Murrone, G. Di Emidio, M. Piccinini, F. Ariu, S. Ledda and C. Tatone, *J. Assist. Reprod. Genet.*, 2013, **30**, 877-882.
13. P. Heraud, K. M. Marzec, Q. H. Zhang, W. S. Yuen, J. Carroll and B. R. Wood, *Sci. Rep.*, 2017, **7**, 8945.
14. M. Ishigaki, Y. Hoshino and Y. Ozaki, *Analyst*, 2019, **144**, 1527-1534.
15. M. Ishigaki, K. Hashimoto, H. Sato and Y. Ozaki, *Sci. Rep.*, 2017, **7**, 43942.
16. T. Takano and R. E. Dickerson, *Proc. Natl. Acad. Sci. USA*, 1980, **77**, 6371-6375.
17. S. Ferguson-Miller, D. L. Brautigan and E. Margoliash, *J. Biol. Chem.*, 1976, **251**, 1104-1115.
18. M. Degli Esposti, S. De Vries, M. Crimi, A. Ghelli, T. Patarnello and

- 1
2
3
4
5
6 A. Meyer, *Biochim. Biophys. Acta, Bioenerg.*, 1993, **1143**, 243-271.
7
8
9
10 19. A. Y. Andreyev, Y. E. Kushnareva, A. A. Starkov, *Biochemistry*, 2005,
11
12 **70**, 200-214.
13
14
15 20. A. Trifunovic and N. G. Larsson, *J. Intern.*, 2008, **263**, 167-178.
16
17
18 21. G. Lenaz, C. Bovina, M. D'aurelio, R. Fato, G. Formiggini, M. L.
19
20
21
22
23
24
25
26
27
28
29
30
31
32
33
34
35
36
37
38
39
40
41
42
43
44
45
46
47
48
49
50
51
52
53
54
55
56
57
58
59
60
- Genova, G. Giuliano, M. M. Pich, U. Paolucci, G. P. Castelli and B.
Ventura, *Ann. N. Y. Acad. Sci.*, 2002, **959**, 199-213.
22. C. Tatone, M. C. Carbone, S. Falone, P. Aimola, A. Giardinelli, D.
Caserta, R. Marci, A. Pandolfi, A.M. Ragnelli and F. Amicarelli, *Mol.
Hum. Reprod.*, 2006, **12**, 655-660.
23. A. P. Goud, P. T. Goud, M. P. Diamond, B. Gonik and H. M.
Abu-Soud, *Free Radic. Biol. Med.*, 2008, **44**, 1295-1304
24. K. R. Dunning, K. Cashman, D. L. Russell, J. G. Thompson, R. J.
Norman and R. L. Robker, *Biol. Reprod.*, 2010, **83**, 909-918.
25. T. Watanabe, A. Thayil, A. Jesacher, K. Grieve, D. Debarre, T. Wilson,
M. Booth and S. Srinivas, *BMC Cell Biol.*, 2010, **11**, 38.
26. P. Haggarty, M. Wood, E. Ferguson, G. Hoad, A. Srikantharajah, E.
Milne, M. Hamilton and S. Bhattacharya, *Hum. Reprod.*, 2006, **21**,

- 1
2
3
4
5
6 766-773.
7
8
9 27. C. Sakai, Y. Hoshino, Y. Sato and E. Sato, *J. Assist. Reprod. Genet.*,
10
11
12 2011, **28**, 157-166.
13
14
15 28. Y. Sugano, M. Yazawa, S. Takino and S. Niimura, *Zygote*, 2016, **24**,
16
17
18 900-908.
19
20
21 29. A. H. Gates, C. H. Donaldson and M. D. Levy, *Teratology*, 1981, **24**,
22
23
24 321-327.
25
26
27 30. Y. Hoshino, and E. Sato, *Dev. Biol.*, 2008, **314**, 215-223.
28
29
30 31. Z. Movasaghi, S. Rehman and I. U. Rehman, *App. Spectrosc.*
31
32
33 *Rev.*, 2007, **42**, 493-541.
34
35
36 32. J. L. Deng, Q. Wei, M. H. Zhang, Y. Z. Wang and Y. Q. Li, *J. Raman*
37
38
39 *Spectrosc.*, 2005, **36**, 257-261.
40
41
42 33. D. D. Lee, Seung, *Nature*, 1999, **401**, 788-791.
43
44
45 34. J. R. Williamson and R. H. Cooper, *FEBS Lett.*, 1980, **117**, 73-85.
46
47
48 35. T. Somfai, M. Kaneda, S. Akagi, S. Watanabe, S. Haraguchi, E.
49
50
51 Mizutani, T. Q. Dang-Nguyen, M. Geshi, K. Kikuchi and T. Nagai,
52
53
54 *Reprod. Fertil. Dev.*, 2011, **23**, 912-920.
55
56
57 36. K. R. Dunning, D. L. Russell and R. L. Robker, *Reproduction*, 2014,
58
59
60

1
2
3
4
5
6 **148**, 15-27.
7

8
9 37. C. Magnusson, T. Hillensjö, A. Tsafiriri, R. Hultborn, K. Ahrén, *Biol.*

10
11
12 *Reprod.*, 1977, **17**, 9-15.
13
14
15
16
17
18
19
20
21
22
23
24
25
26
27
28
29
30
31
32
33
34
35
36
37
38
39
40
41
42
43
44
45
46
47
48
49
50
51
52
53
54
55
56
57
58
59
60

Author contributions

M.I. and Y.H. designed the experiments. Y.H. performed animal surgery and treated the embryo culture. M.I., S.K., and S.W. carried out the Raman measurements and data analysis. M.I. drafted the manuscript, and all the authors approved the manuscript for publication.

Acknowledgments

This work was supported by the JSPS project of the Leading Initiative for Excellent Young Researchers (M.I.), JSPS KAKENHI Grant Number 19K06369 (Y.H.), and Adaptable and Seamless Technology transfer Program through Target-driven R&D (A-STEP) from JST Grant Number JPMJTR21447297 (M.I. and Y.H.).

Conflicts of interest

There are no conflicts to declare.

Table 1: Peak assignments for Raman spectra obtained for mouse oocytes.

Peak (cm ⁻¹)	DNA/RNA	proteins	lipids
742		sym ring br of Try	
747		cytochromes	
828	asym str PO ₂ ⁻	ring br Tyr	
850		ring br Tyr	
1001		sym ring br Phe	
1126		C-N str, cytochromes	
1242	T, A	Amide III	=C-H ben
1311-1337		CH ₃ /CH ₂ twi, ben, cytochromes	CH ₃ /CH ₂ twi, ben
1445		CH def	CH def
1582		cytochromes	
1656		Amide I	C=C str

Abbreviation: br: breathing, str: stretching, twi: twisting, ben:

bending, def: deformation, sym: symmetric, asym: asymmetric

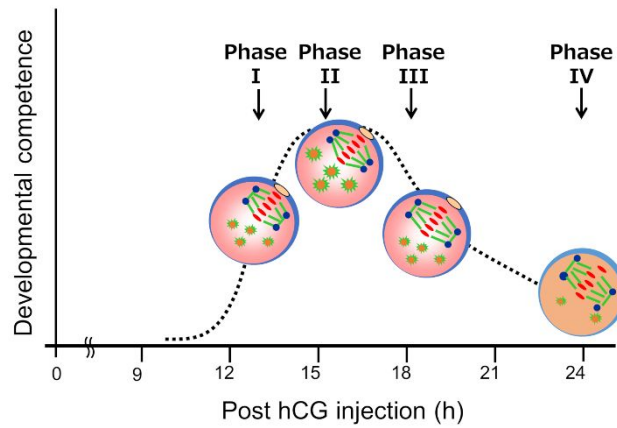


Figure 1: Variation in developmental competence over the course of oocyte maturation. In oocyte with high DC, the pericentriolar materials (PCM) distance between the spindle poles is short and increasing over time. In addition, the expression of microtubule organizing center in the cytoplasm also becomes strong when PCM is approaching.

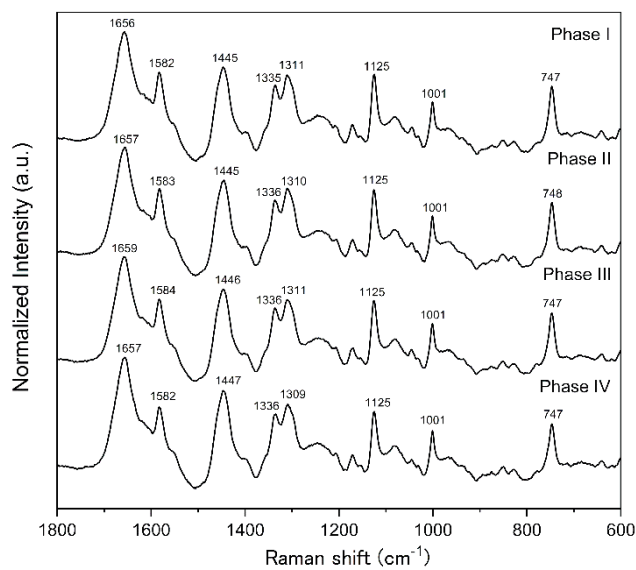
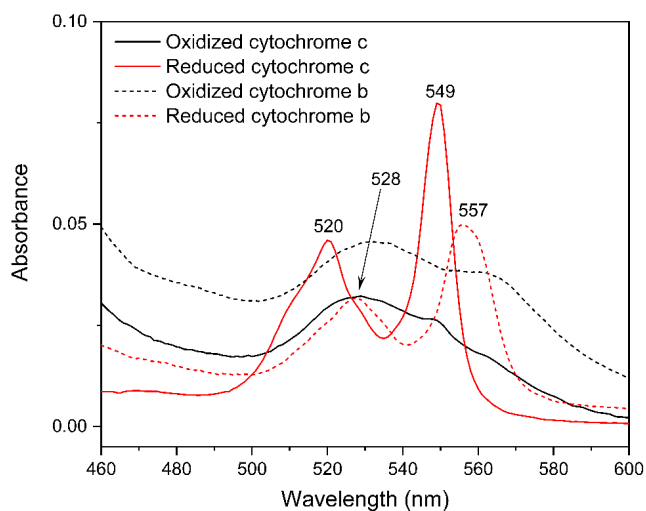


Figure 2: Averaged Raman spectra in 1800–600 cm⁻¹ region for mouse oocytes obtained at Phases I (n=44), II (n=58), III (n=59), and IV (n=57).

(A)



(B)

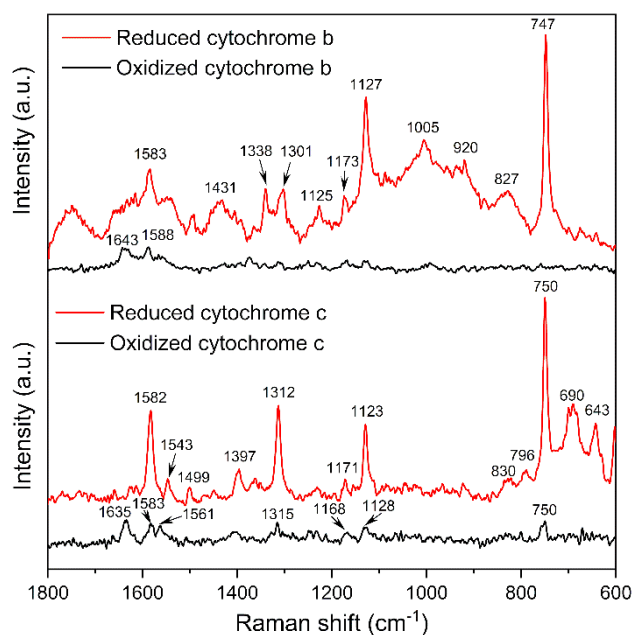
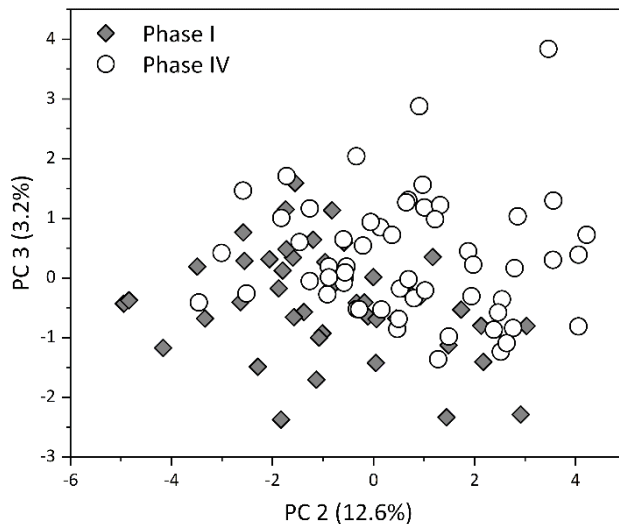
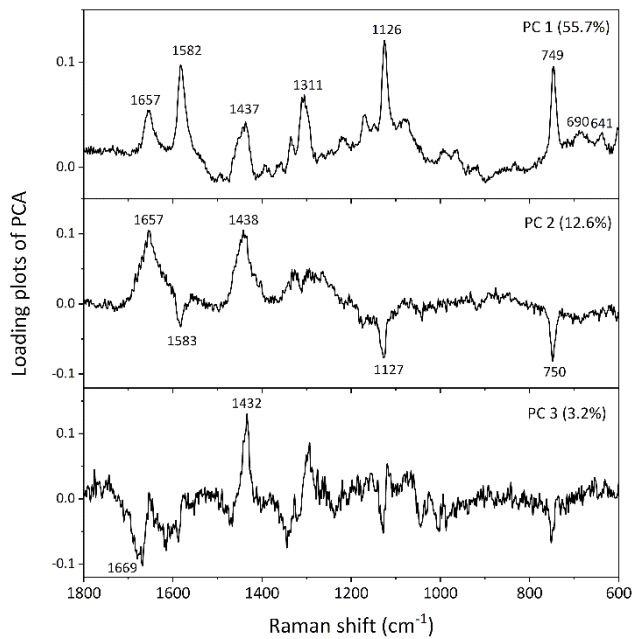


Figure 3: (A) UV-Vis absorbance spectra (460-600 nm) and (B) 532-nm-excited Raman spectra (1800-600 cm^{-1}) of oxidized and reduced cytochrome *b* and *c*.

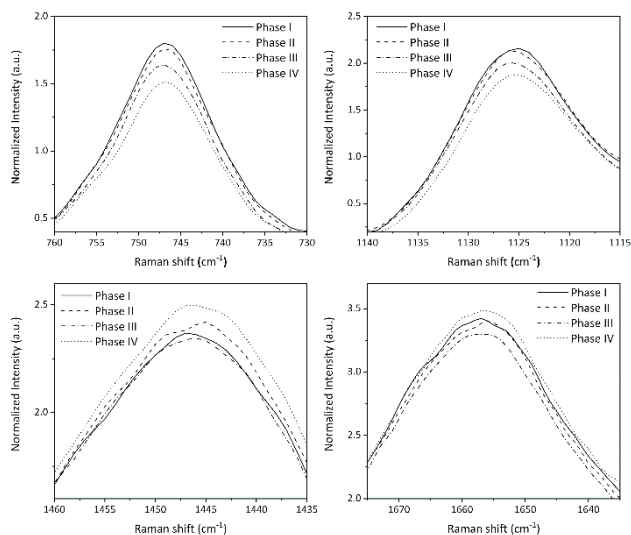
(A)



(B)



(C)



(D)

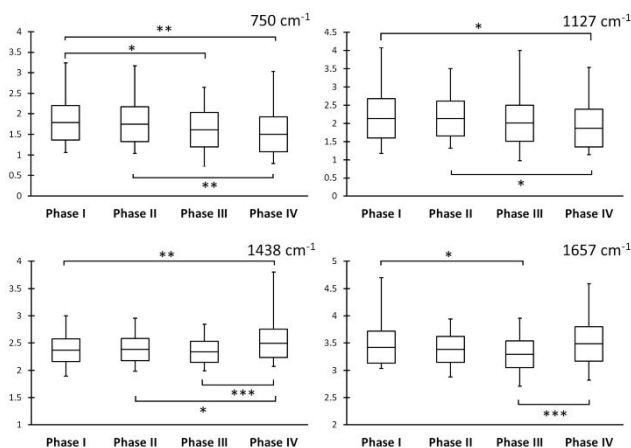
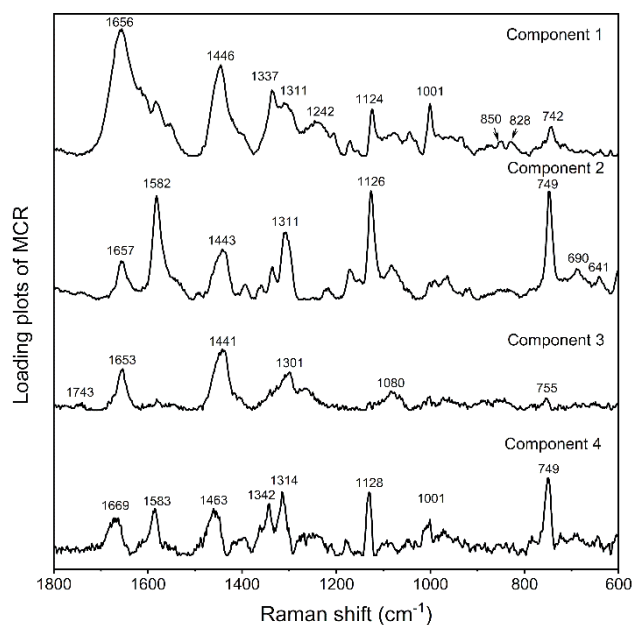


Figure 4: (A) Score plots of PC2 vs PC3 obtained by PCA; (B) loading plots of PC1, PC2, and PC3 obtained by PCA; and (C) comparison of spectral intensities and (D) the corresponding variations of these intensities at 748, 1127, 1442, and 1652 cm⁻¹ for Phases I, II, III, and IV. Box plots in (D) are expressed as mean value \pm standard deviation (SD), where

1
2
3
4
5
6 central line is mean value, and error bars show range between minimum
7
8
9 and maximum values; significant differences were assessed by *t*-test (*:
10
11
12 $p < 0.05$, **: $p < 0.01$, ***: $p < 0.001$).

(A)



(B)

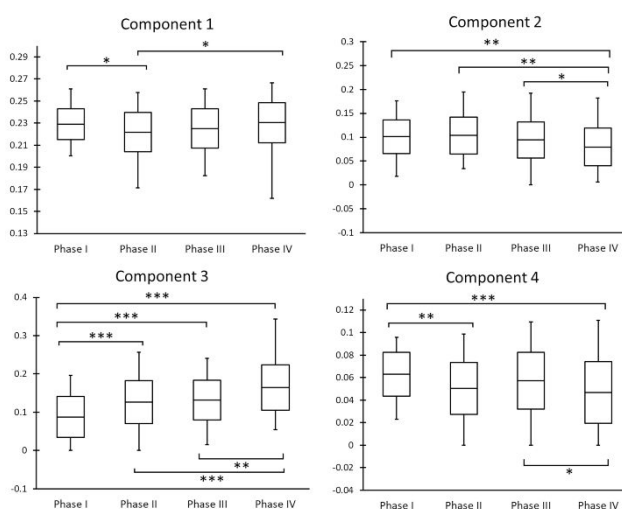
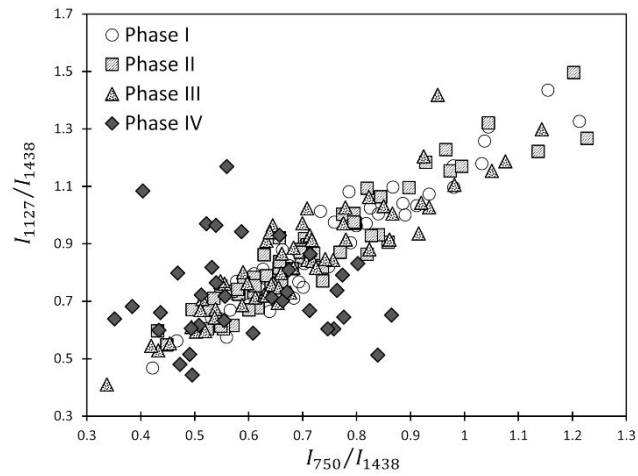


Figure 5: (A) Spectra of pure components and (B) corresponding variations in concentration extracted by MCR: box plots in (B) are expressed as mean value \pm standard deviation (SD), where central line is mean value, and error bars show range between minimum and maximum values; significant

1
2
3
4
5
6 differences were assessed by *t*-test (*: $p < 0.05$, **: $p < 0.01$, ***: $p < 0.001$).
7
8
9
10
11
12
13
14
15
16
17
18
19
20
21
22
23
24
25
26
27
28
29
30
31
32
33
34
35
36
37
38
39
40
41
42
43
44
45
46
47
48
49
50
51
52
53
54
55
56
57
58
59
60

(A)



(B)

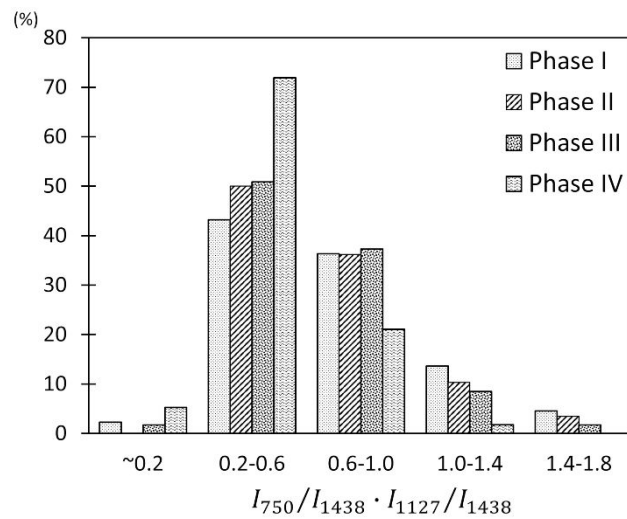
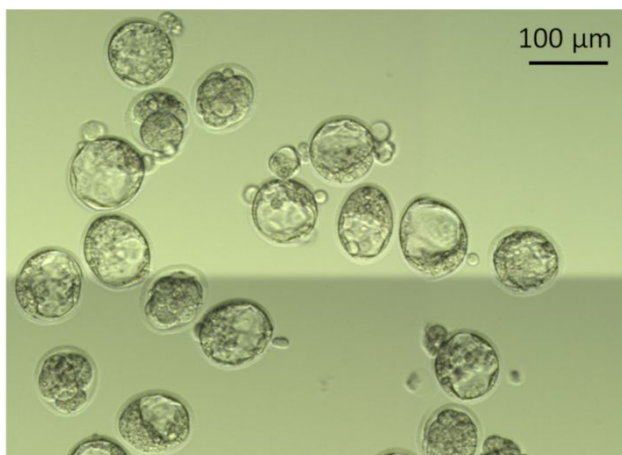


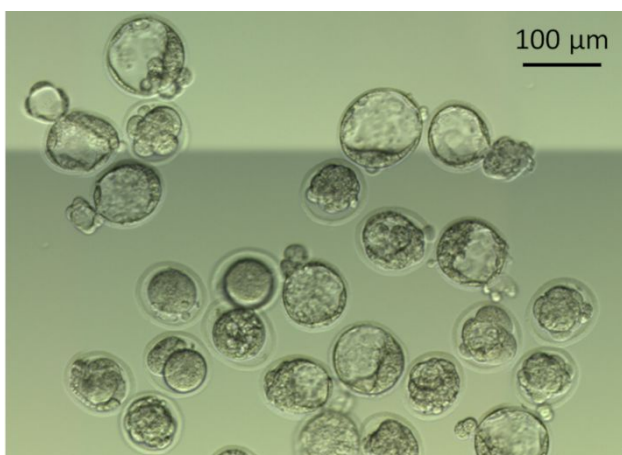
Figure 6: (A) Score plot of I_{750}/I_{1438} vs I_{1127}/I_{1438} and (B) frequency distribution of product of I_{750}/I_{1438} and I_{1127}/I_{1438} .

1
2
3
4
5
6
7 (A)
8
9



30
31
32
33
34
35
36
37
38
39
40
41
42
43
44
45
46
47
48
49
50
51
52
53
54
55
56
57
58
59
60

(B)



(C)

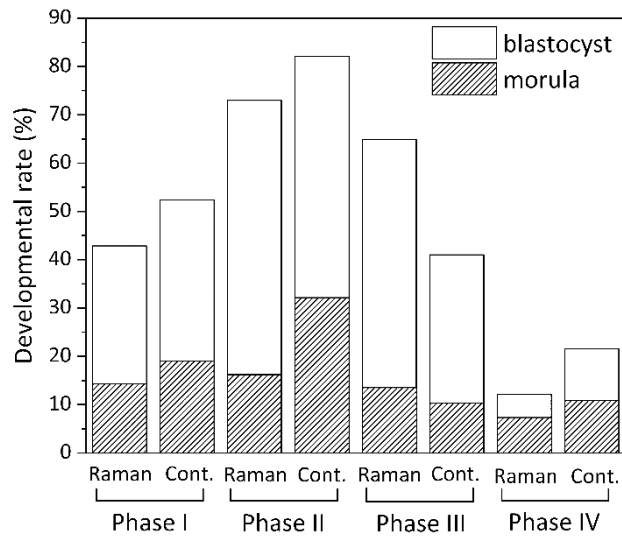


Figure 7: Image of embryos on 5th day of incubation: (A) laser-irradiated and (B) nonirradiated embryos; (C) developmental rates (%) of oocytes that progressed to morula or blastocyst stages.